Magnetic configurations of Co(111) nanostripes with competing shape and crystalline anisotropies

Yu. P. Ivanov,[1,2] O. Iglesias-Freire,[1] E. V. Pustovalov,[2] O. Chubykalo-Fesenko,[1] and A. Asenjo[1]
[1]*Instituto de Ciencia de Materiales de Madrid, CSIC, Cantoblanco, 28049 Madrid, Spain*
[2]*Far Eastern Federal University, 690950 Vladivostok, Russia*
(Received 30 October 2012; published 10 May 2013)

Nanostripes with varying widths are lithographed on Co thin films with strong magnetic anisotropy resulting from the epitaxial growth onto vicinal Si(111) substrate. The competition between magnetocrystalline and shape anisotropies is used to tune the magnetic behavior of Co nanostripes. Single domain configuration is observed for nanostructures where magnetocrystalline and shape anisotropies go along the same direction. However, more complicated configurations such as open stripe domains can be developed when both anisotropies compete. The nanostructures have been experimentally characterized by longitudinal magneto-optical Kerr effect and magnetic force microscopy (MFM). Micromagnetic simulations performed by finite-element and finite difference codes are in good agreement with the experimental results. The use of MFM based techniques such as the variable field magnetic force microscopy and the so-called three-dimensional modes has allowed us to follow the evolution of the domains and domain walls under externally applied magnetic fields, i.e., to deeply understand the magnetization reversal process in the multidomain nanostripes. In particular, the nanostripes with competing anisotropies and a high aspect ratio present vortex configuration along the domain walls which have a key role in the magnetization reversal process.

DOI: 10.1103/PhysRevB.87.184410 PACS number(s): 75.75.−c, 75.30.Gw, 68.37.Rt, 75.78.Cd

I. INTRODUCTION

Modern lithography technology such as focused ion-beam etching has allowed the fabrication of nanoscale magnetic structures potentially useful for data storage, logic devices, and sensors.[1,2] In particular, possible applications of magnetic nanowires (NWs) include magnetic racetrack memories,[3] domain-wall logic devices,[2] and magnonic crystals.[4] The main interest of these one-dimensional elements resides in the possibility to control the magnetic structure via its confinement for dimensions of the order of the magnetic correlation length. The most significant feature of nanowires is that the magnetization reversal by means of the domain wall (DW) propagation can be controlled using magnetic field and electric current.[5–7]

Over the past decade, many studies have focused their attention on establishing a phase diagram of the possible domain structures as a function of the nanowires aspect ratio.[8] Most of the previous works investigate polycrystalline NWs, for example, based on permalloy (Py), where the shape anisotropy always dominates the magnetization reversal processes. To increase the efficiency of spin transfer torque effect in NWs it is necessary to use materials with large magnetocrystalline anisotropy.[9] Several experiments were performed on monocrystalline Co(1010),[10] Fe(110),[11,12] and CrO_2(100) (Ref. 13) nanostructures with intrinsic uniaxial in-plane crystalline anisotropy. Magnetocrystalline anisotropy can be also achieved, for example, by oblique evaporation along different azimuthal angles.[14] Long magnetic nanowires also present shape anisotropy with the strength defined by the width-to-length ratio. The competition between magnetocrystalline anisotropy, shape anisotropy, and exchange energy in monocrystalline NWs produces much richer behavior than that observed in polycrystalline NWs of Py.[10] Different magnetic configurations have been found in NWs with competing anisotropies: longitudinal single domain, transverse single domain, or stripe domain structures with flux closure domains. The dynamical origin of stripe domains has been established as resulting from the lowest frequency spin-wave mode.[15] However, the exact structure of the DWs and their evolution during magnetization processes were never discussed and remain open. The detailed spin distribution in the wall is important because it affects the nature and strength of the pinning effects[16] in the devices based on the controlled DW motion or the ones based on DWs stray field such as for sensing convey atoms[17] and magnetic molecules.[18,19] In other possible applications DWs may act as remote mobile pinning centers for other DWs,[20] as well as for stabilizing other magnetic states, for example, in ring structures.[21]

In this paper we have prepared Co nanostripes with internal magnetocrystalline anisotropy originated from the epitaxial growth onto vicinal Si(111) substrate.[22] The stepped silicon surface used as templates tries to maintain the preferred orientation, but is forced by the miscut to form atomic steps separated by atomically flat terraces. Co(111) ultrathin films deposited on such substrate by molecular beam epitaxy (MBE) present strong uniaxial anisotropy.[22] The nanostripes are then created by lithography techniques to produce a competing effect between crystalline and shape anisotropies. We show that the magnetocrystalline anisotropy produced by the vicinal monocrystal substrate is strong enough to compete and even to completely overcome the shape anisotropy. We have studied the magnetic domain structure and the domain walls in the nanostripes by longitudinal magneto-optical Kerr effect (LMOKE) and magnetic force microscopy (MFM) at room temperature (RT). The complimentary micromagnetic simulations are also performed using the finite-element MAGPAR code[23] and the finite difference OOMMF code.[24] Variable field magnetic force microscopy (VF-MFM)[25] and the three-dimensional (3D) mode MFM-based technique[26] combined with the micromagnetic simulations allow us to produce a reliable understanding of the internal spin structure. By varying the width of the nanostripes and its orientation

with respect to the stepped surface, the overall magnetic anisotropy—consisting of the magnetocrystalline and the shape anisotropy—can be controlled. The compensation point between both anisotropies is determined. We have characterized the magnetic domains and domain wall configurations and shown the role of the vortex in the magnetization process.

II. SAMPLE PREPARATION

Epitaxial Co(111) films were grown on vicinal Si(111) substrates with 4^0 miscut by MBE in an Omicron ultrahigh-vacuum (UHV) system with a base pressure of 3×10^{-11} Torr. Scanning tunneling microscopy (STM) observations revealed a regularly stepped surface with the width of the atomic terraces about 30 nm and steps height 1.5 nm. Prior to Co deposition, the Cu buffer layer was formed on Si(111) surface to prevent intermixing of Co and Si and to smooth the mismatch of Co and Si lattice parameters. The epitaxial layer-by-layer-like growth of Cu(111) on Si(111) is observed only up to 2.4–2.8 nm of Cu.[27] The best crystalline quality of Co(111) films corresponds to the 2-nm Cu(111) buffer layer.[22] Since the Co layer is forced to form atomically flat terraces separated by atomic steps, the magnetic film presents strong uniaxial anisotropy along the step direction.[22] The thickness of Co films was 10 nm.

In order to obtain magnetic nanostructures with controlled anisotropy, the epitaxial Co(111) surface has been patterned by focused ion-beam (FIB) milling. Removal of magnetic material has been produced by focused ion-beam Ga+ with energy of 30 kV and a current of 0.1–1.0 nA. Two series of nanostripes have been prepared with the main axis oriented either parallel [Fig. 1(b)] or perpendicular [Fig. 1(c)] to the steps of the Co epitaxial film. In the following, the nanostripes aligned parallel to the steps, i.e., parallel to the easy axis direction of the Co(111) film, will be called PAR while the nanostripes oriented perpendicularly to the step direction will be called PER. The widths of the two series of nanostripes as well as the corresponding labels are collected in Table I.

To reduce the roughness and to increase the sharpness of the boundaries between the magnetic material (nanostripes) and the nonmagnetic area, the ion-beam scanning at high frequency, a few kilohertz, was used and the sides of the

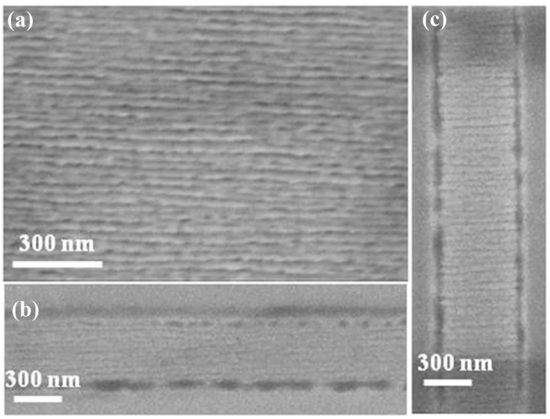

FIG. 1. SEM images of (a) stepped Co(111) surface, (b) PAR nanostripe with the main axis parallel to the Co steps, and (c) PER nanostripe with the main axis perpendicular to the Co steps.

TABLE I. Width of the two series of nanostripes prepared from the stepped Co thin film. The length of all nanostructures is 50 μm.

Width (nm)	PAR	PER
150	PAR150	PER150
300	PAR300	PER300
450	PAR450	PER450
550	PAR550	PER550
750	PAR750	PER750
850	PAR850	PER850
1000	PAR1000	PER1000
1500	PAR1500	PER1500
2000	PAR2000	PER2000

nanostripes were parallel to the scanning lines. The SEM images have shown very sharp edges of the nanostripes (Fig. 1). The FIB is known to alter the magnetic properties close to the nanostripe edge due to Ga ions implantation.[28] However, in our case this effect is negligible. The MFM study did not show any significant changes in the magnetic properties in the region close to the edges. At the same time, because of the stepped film surface, the geometrical defects with the size of terrace width are observed at the edges [Figs. 1(b) and 1(c)]. The effect of such defects on magnetic properties of nanostripes will be discussed in Sec. V.

III. HYSTERESIS LOOPS OF INDIVIDUAL NANOSTRIPES

A. Hysteresis loops of PAR and PER nanostripes by LMOKE and simulations

The hysteresis loops of epitaxial Co(111) nanostripes have been obtained by LMOKE. Data corresponding to PAR750 and PER750 nanostripes are shown in Fig. 2. Hysteresis loops measured along the main axis in PAR nanostripes present rectangular shape as shown in Fig. 2(a). However, unhysteretic behavior is found when the magnetic field is applied perpendicular to the main axis [see Fig. 2(b)]. PAR nanostripes exhibit uniaxial anisotropy, independently on their width, i.e., it is expected that after in-plane saturation along the main axis they present single domain configuration. However, PER nanowires exhibit more complex behavior due to the competition between magnetocrystalline anisotropy (perpendicular to the NW axis) and shape anisotropy (dependent on the nanostripes geometry). Therefore, the value of the magnetocrystalline anisotropy, induced by the vicinal monocrystal substrate, is strong enough to overcome the shape anisotropy. The magnetization reversal process and the domain configuration strongly depend on the width of the nanostripes and on the applied magnetic field direction [see Figs. 2(c) and 2(d)].

To understand the magnetic behavior of both nanostripes series, we have performed a micromagnetic simulation by the finite-element MAGPAR code. The following parameters have been used to simulate nanostripes: length $l = 1000$–7000 nm, width $w = 100$–700 nm, fixed $l/w = 10$, thickness $t = 10$ nm, magnetocrystalline anisotropy constant $K = 6.3 \times 10^4$ J/m^3, exchange stiffness $A = 13 \times 10^{-12}$ J/m, saturation magnetization value $M_s = 1.75$ T, and a mesh of 5 nm. The magnetocrystalline anisotropy constant was obtained from the experimental hysteresis loops measured by vibrating sample

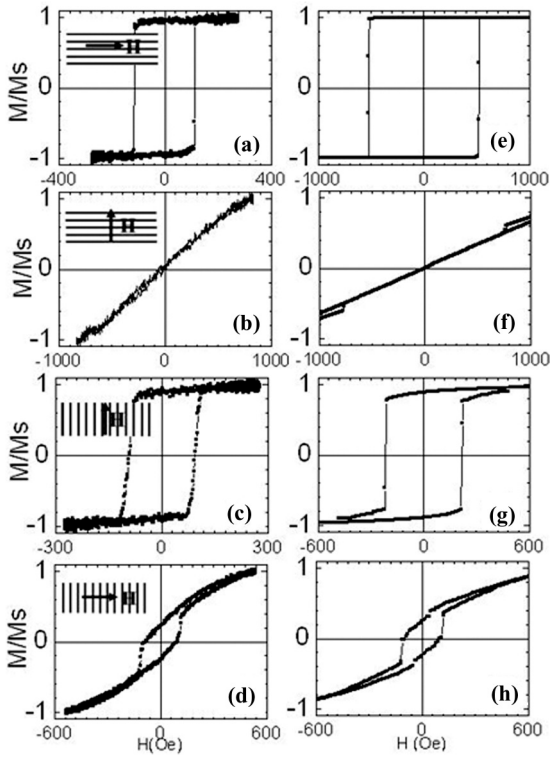

FIG. 2. Experimental (a)–(d) and simulated (e)–(h) hysteresis loops for the nanostripes PAR750 [(a), (b), (e), and (f)] and PER750 [(c), (d), (g), and (h)]. The orientation of NW axis, surface steps, and the direction of the applied magnetic field are shown in insets.

magnetometrer on epitaxial Co films. Due to high crystallinity of Co films, a typical saturation magnetization value for Co was used. The simulated hysteresis loops are shown in Figs. 2(e)–2(h). Our calculations are qualitatively in agreement with the experimental data although, in general, the simulated critical fields are larger than the experimental ones. Such discrepancy between the experimental and modeled values is expected and is attributed to the presence, in the real samples, of defects and possible small mismatch between vicinal steps and the orientation of lithographed nanostripes.[29]

Experimental and theoretical results corresponding to all prepared samples (see Table I) have been collected in Fig. 3, where we present the dependence of the coercivity on the inverse nanostripe width. In PAR nanostripes the coercive field along the easy axis increases linearly when the width decreases. On the other hand, when the magnetic field is applied perpendicularly, the coercivity values remain practically zero. As usual, micromagnetic modeling overestimates the value of the coercive field due to an idealized character of the model material.[29] Despite the higher values, there is a good agreement between the experiment and simulations which serves as a validation of the model.

In order to get an insight into the coercivity behavior of PAR nanostripes, simple analytical estimations are useful. Since the ratio length/width/thickness ($l/w/t$) is varied from 5000/15/1 to 5000/200/1, the demagnetization fields can be calculated in the approximation for the two-dimensional problem. For magnetization along the nanostripe axis the corresponding demagnetization factor is $N_l \sim 2t/\pi l$ and for the magnetization perpendicular to the nanostripe is $N_w \sim 2t/\pi w$.[30] The shape anisotropy field is proportional to the difference in the demagnetization fields in two orthogonal directions $H_{sh} = M_s(N_l - N_w) \sim (2t/\pi w)(w/l - 1)$. Since the ratio is $w/l < 0.1$ for all the nanostripes presented in this work, the resulting shape anisotropy field H_{sh} is inversely proportional to the nanostripe width. In agreement with this analysis, we have demonstrated that the coercivity of PAR nanostripes with the field applied parallel to their easy axis is inversely proportional to the width (see Fig. 3), reflecting the shape anisotropy dependence. However there is a transition region around $w = 300$ nm, where we can observe both in the experiment and calculations a change in the slope. Notice that the simple demagnetizing factor approach is only valid for the demagnetization process based on coherent reversal and ellipsoidal samples. The real magnetostatic fields are not uniform across the nanostripe. For a complete understanding, micromagnetic simulations which do not use the approximation of the shape anisotropy demagnetizing factors should be used.

In the case of PER series, magnetocrystalline and shape anisotropies compete. The strong magnetocrystalline anisotropy dominates the magnetic behavior for wide nanostripes that present overall anisotropy along the NW, while the shape anisotropy becomes more important for narrower structures. A transition region occurs at around 400–600 nm where LMOKE parallel and perpendicular hysteresis loops have similar squarenesses. For PER450 nanostripe the ratio of the remanent to the saturation magnetization in the case of

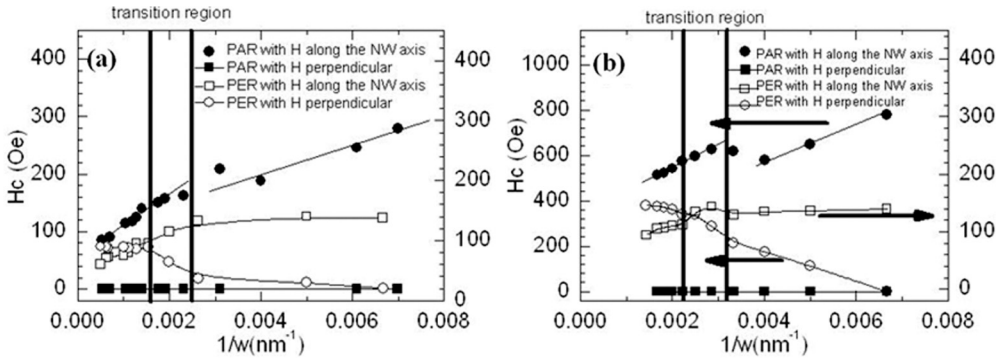

FIG. 3. The dependence of coercivity on the inverse nanostripes width: (a) experimental data, (b) micromagnetic simulations. The vertical lines indicate the compensation region for PER nanostripes at which hysteresis cycles do not show the pronounced presence of uniaxial anisotropy.

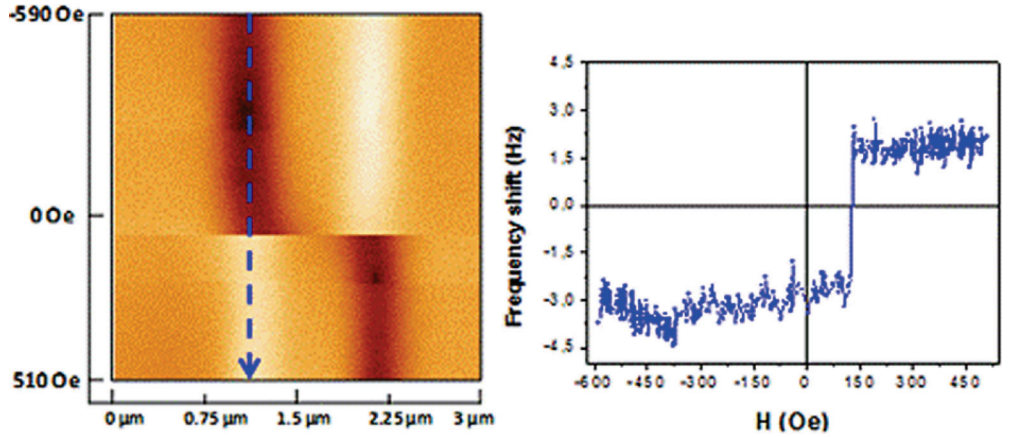

FIG. 4. (Color online) 3D-mode image performed in PER750 nanostripe. The magnetic field is swept between − 590 and 510 Oe.

magnetic field applied parallel to the long side of nanostripe (the easy direction of the shape anisotropy) and parallel to the direction of the steps (the easy direction of the magnetocrystalline anisotropy) is 0.49 and 0.44, accordingly, which corresponds to practically full compensation of the anisotropies. The decrease of the perpendicular coercive field with the nanowire width below the transition region demonstrates that the overall anisotropy starts to be directed parallel to the short length and reflects the increase of the shape anisotropy, decreasing the overall one. The wide nanowires in this case have coercive fields almost independent on their width. As is well known (see, for example, Ref. 31) when the field is applied perpendicular to the nanostripe, nonhomogeneous magnetostatic fields produce "closure" domains at the remanence. In this case, close to the nanostripe edges, magnetization is parallel to the long direction, staying perpendicular to it inside the nanostripe. Once these closure domains are fitted inside the nanostripe, the coercive field is only determined by the magnetization rotation in the inner region and is independent on the nanostripe width, as was reported preciously for Fe nanowires.[31]

For narrow PER stripes the coercive field along the main axis direction is also practically independent from the width, different from what was observed in PAR nanostripes. This happens due to the separation in magnetic domains along nanostripes, which produces minimization of the magnetostatic energy.

The key for the detailed explanation of the behavior of the coercivity in nanostripes resides in understanding the changes in these domains (i.e., magnetization reversal modes) as a function of nanostripe width. This will be done in Secs. IV and V, where we show that the change of demagnetization processes is due to the appearance of different magnetization configurations. Since this will be done using the VF-MFM, first we also measure the hysteresis processes using this local technique and discuss the differences with LMOKE measurements.

B. Local hysteresis loops of individual PER nanostripes by VF-MFM

Local hysteresis loop measurements were performed using a MFM from Nanotec Electronica™.[32] Such a system, working in a noncontact mode, allows us to acquire simultaneously the topography of the surface and the magnetic force gradient map. By using the so-called VF-MFM technique[25] the reversal process of Co(111) nanowires has been studied. A recently developed technique[26] has been used in which a nonstandard MFM picture is obtained by continuously scanning the same profile (horizontal axis), as the magnetic field (vertical axis) is swept smoothly, as shown in Fig. 4(a). As a result, these images yield information about the magnetic structure along this profile for the whole range of the applied fields. Special MFM tips have been fabricated for this study by coating standard atomic force microscopy (AFM) nanosensor probes with a Co thin film. The accurate thickness has been chosen to avoid irreversible changes on the magnetic state of the sample due to the stray field coming out from the tip.[33]

Since the external field is varied in a continuous way, a precise quantification of some critical fields on individual nanostructures can be performed. For statistical purposes, measurements using this so-called 3D-mode were repeated ten times on every structure and the resulting switching fields and their comparison with the LMOKE values are presented in Table II.

VF-MFM measurements are qualitatively in agreement with the LMOKE data corresponding to the wider nanostripes although the critical fields measured by VF-MFM are larger than the LMOKE ones. Such discrepancy is especially important for the narrowest nanostripes case that presents a complex spin configuration far away from the single domain configuration displayed by the wider nanostripes. Notice that

TABLE II. The coercive field Hc obtained by VF-MFM for some nanostripes in the middle of the nanostructure and the LMOKE data corresponding to an average of 100 loops. The magnetic field is applied along the short axis.

Nanostripe	$H_{c\text{-VFMFM}}$ average (Oe)	$H_{c\text{-LMOKE}}$ average (Oe)
PER750	107 ± 15	85 ± 5
PER1000	98 ± 15	91 ± 2
PER1500	96 ± 15	93 ± 2
PER2000	99 ± 15	94 ± 3

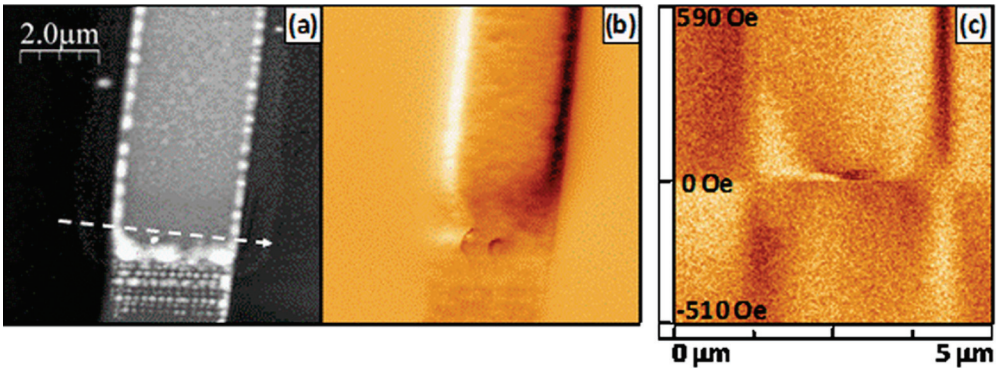

FIG. 5. (Color online) (a) Topography of the edge of the PER2000 nanostripe. (b) MFM image corresponding to the same sample. (c) 3D mode image obtained along the profile marked with a dashed line in (a) when the magnetic field is swept from $+590$ to -510 Oe.

the VF-MFM measurements correspond to the center of the nanostripe while the LMOKE data are the average of 100 loops measured along nearly the whole structure. To further analyze this behavior we have repeated the same kind of 3D mode measurements at the edge of the nanostripes.

The regions very close to both edges present defects that promote the nucleation of domain walls. Figures 5(a) and 5(b) show the topography and the magnetic configuration of the extreme of PER2000 nanostripe. In order to confirm experimentally the nucleation and propagation of domain walls, a 3D-mode measurement was performed very close to the nanostripe end [white arrow on Fig. 5(a)], yielding the picture of Fig. 5(c). For high applied fields, the typical bright-dark contrast associated to the single-domain state can be observed [upper part of Fig. 5(a)]. As can be deduced by the appearance of some contrast in the center of the stripe, for low external fields a domain wall is nucleated until it suddenly disappears (corresponding to the fast propagation of the wall), provoking the magnetization reversal and a reversed contrast on the image. Comparing to the switching field value obtained by VF-MFM in the center of the stripe, here the coercive fields are much smaller. The local character of the MFM can explain the observed difference between the average value obtained by LMOKE and the VF-MFM data.

IV. DOMAIN CONFIGURATION OF PER NANOSTRIPES

The knowledge of the domain and domain wall structures in PER nanostripes is important for the deep understanding of the magnetization reversal process in these nanostructures. In order to clarify the transition between different magnetization configurations in PER nanostripes as a function of their widths, the remanent domain configurations after saturating the sample along the main axis of the stripes were studied by MFM and micromagnetic simulations. As can be seen in Fig. 6, the nanostripes at the remanence can present three different domain structures depending on their width.

In the case of the narrowest structures (PER450) a chesslike configuration is present [see Fig. 6(a)]. This configuration corresponds to the open stripe (OS) spin structure, calculated by the micromagnetic simulations; see Fig. 6(e). In the previous work[10] this kind of domain distribution showed a sudden jump of the magnetization with no intermediate region; here a smooth contrast change between adjacent domains can be observed. In contrast to the statements given in the aforementioned work, the magnetization does not seem to lie completely along the short side of the stripe forming domains separated by well-defined domain walls but rather forms a kind of canted domain between which a smooth domain wall is present [see Fig. 6(a)]. This is in agreement with the measured hysteresis loops where no well-defined easy axis seems to be present. The ratio of the remanent to the saturation magnetization in the case of magnetic field applied parallel and perpendicular to the NW axis is 0.49 and 0.44, accordingly. The magnetocrystalline anisotropy and the shape anisotropy compensate each other. In addition, it is worth pointing out that some features due to the irregular topography are present in the MFM images, especially two protuberances on both sides of the stripes [visible in Fig. 5(a)]. These features give rise

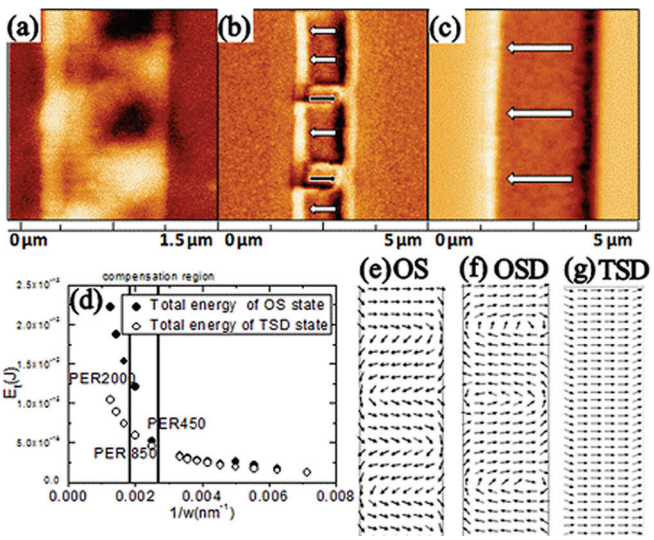

FIG. 6. (Color online) MFM images obtained in remanent state after saturating nanostripes along the main axis: (a) PER450, (b) PER850, (c) PER2000 nanostripes. (d) Calculated dependence of the total energy of open stripe domains and transverse single domain states on the nanostripe width. The lines show the boundaries of the compensated region. Figures 6(e)–6(g) show the spin configurations for OS, OSD, and TSD magnetic states, accordingly, calculated from micromagnetic simulations. The contrast of the MFM images is (a) 2.43 Hz, (b) 2.80 Hz, and (c) 8.98 Hz.

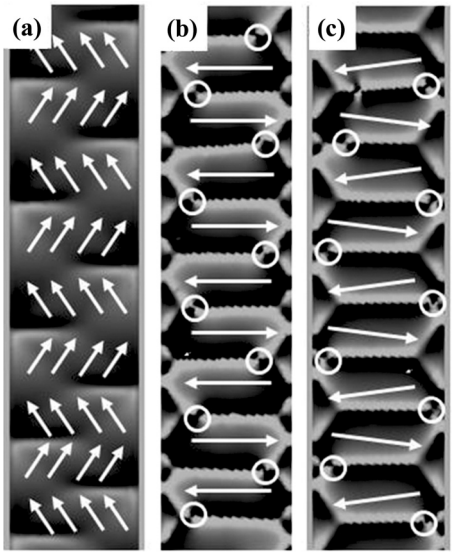

FIG. 7. Simulated micromagnetic configurations for PER550 nanostripe for different values of the magnetic field applied parallel to the nanostripe long axis: (a) OS state: $H = 500$ Oe; (b) OSD state at the remanence; (c) OSD state near the coercivity. The arrows indicate the average magnetization direction, the color is the divergence of the magnetization vector (simulated MFM contrast), and the open circles are the position of vortex in DWs.

to a slight bright contrast which should not be interpreted as resulting from the magnetostatic interaction.

For the case of intermediate widths a different configuration is observed, in which the lower energy cost associated to the magnetostatic energy favors the formation of well-defined domains with magnetization in the center perpendicular to the stripe and aligned parallel to it at the borders ("open stripe domain," OSD state). As can be clearly seen in Fig. 6(b), these domains are separated by well-defined domain walls. Unlike previously reported results,[13] our Co(111) nanostripes do not present a flux-closure stripe domain state due to a stronger value of the uniaxial magnetocrystalline anisotropy. Note that the OS [Fig. 6(e)] and the OSD [Fig. 6(f)] states are similar and there is a continuum transition between them as the width increases. The difference is that in the second case the corresponding inhomogeneous magnetization structures fit completely inside the nanostripe and, consequently, present a better contrast (see the simulated MFM images in Fig. 7). Inside the OSD state a vortex is formed. Some small asymmetry in the configuration in Fig. 6(b) could be attributed to two main reasons. First, it may be due to the presence of possible distribution of magnetocrystalline anisotropy along the nanostripe, the presence of defects, and a small deviation of up to few degrees of the external field from the stripe main axis, resulting in a dependence of the domain size on the field direction. Second, for the geometrical parameters corresponding to Fig. 6(b) the TSD state has lower energy than the OS (OSD) state meaning that the OSD state is a metastable configuration. Consequently, part of the nanostripe (depending again on local conditions) can be in the TSD state.

In the case shown in Fig. 6(c), nanostripes with large widths show quasi-single-domain behavior [transverse single domain (TSD) configuration; see the micromagnetic simulations in Fig. 6(g)], i.e., the magnetization points along the same direction in regions which are tens of microns long. Here the magnetocrystalline anisotropy widely overcomes the magnetostatic energy resulting in single domain areas comprising the vast majority of the stripe.

The total energy of the OS (OSD) and the TSD states calculated from the micromagnetic simulation is shown on Fig. 6(d) as a function of the nanostripe width. For narrow nanostripes the multidomain configuration is favorable in agreement with the image for the PER450 stripe; while increasing the width the single domain state is stabilized (as imaged for the PER2000 stripe). The boundary between the TSD and OS states is similar to what has been calculated from the domain theory model based on Kittel's formulation for Co(0001) nanowires.[10] For nanostripes in the compensation region, the energy associated to a single-domain structure is very similar to that needed to split it into a multidomain configuration, and, thus, we can expect the occurrence of one or another state in different regions of the same nanostripe as observed for PER850.

Notice that the stable magnetic configurations shown above correspond to the extensive central area of the stripes. The regions very close to both edges show a different behavior and will be discussed next.

In conclusion, the transition between different domain configurations (Fig. 6) explain different coercivity behavior in three regions presented in Fig. 3. The numerical and experimental results are in good agreement which serves as a support of our conclusions.

V. DOMAIN WALLS ON PER NANOSTRIPES

A. Nature and role of domain walls on PER nanostripes

Domains of different types lead to different demagnetization processes. For complete understanding of the physical mechanisms, it is necessary to study the evolution of the magnetization structure under the applied field.

Figure 7 presents the results of the micromagnetic simulations showing the corresponding configurations and the simulated MFM images for a PER nanostripe geometry at different magnetic fields applied parallel to the nanostripe long axis. The magnetization reversal starts from forming a periodic domain structure, i.e., OS state [Fig. 7(a)], then 180 Néel domain walls (DWs) separating stripe domains (OSD state) are formed. Near the remanent state vortices nucleate in DWs [Fig. 7(b)]. At the coercivity field all vortices move rapidly to the opposite edge of the nanostripe. Note that the vortices in the neighboring DWs have opposite chirality and, consequently, move to the opposite edges of the NW, perpendicular to the direction of the magnetic field. After vortex motion, the simulated MFM contrast of DWs is switched [Fig. 7(c)]. Also during the vortices motion new domains can be formed.

The first important prediction of the micromagnetic simulations is the presence of the vortex in domain walls. These predictions are confirmed by VF-MFM imaging in wide PER nanostripes. For wide stripes and fields near the coercive field values, single or double vortex DWs can be formed. In Fig. 8, high-resolution MFM images and the results of the

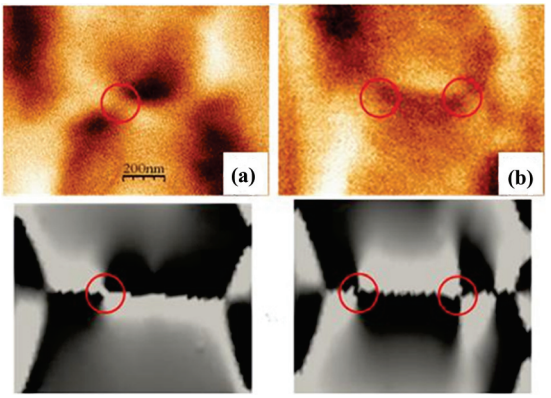

FIG. 8. (Color online) High-resolution MFM images (up) and results of micromagnetic simulation (down) for vortex (a) and double vortex (b) DWs in PER850 nanostripe.

micromagnetic simulation showing the vortex [Fig. 8(a)] and the double vortex [Fig. 8(b)] DWs are presented.

However, the good agreement between the simulation and the MFM data extends further than the existence of vortex in the DW to the general mechanism of the magnetization process deduced from both methods. Figure 9 shows a series of MFM images measured, after saturating the sample, under an external magnetic field applied parallel to the long axis of the PER850 nanostripe. By reducing the magnetic field, a quasiperiodic (OSD) domain structure is achieved [Fig. 9(a)]. At lower magnetic fields Néel domain walls and vortex nucleate [Fig. 9(b)]. This configuration is stable up to around 160 Oe [Figs. 9(c) and 9(d)]; for lower magnetic fields the contrast of the walls changes, as we can observe comparing the images in Figs. 9(d) and 9(e). This field corresponds to the coercive field where, according to the simulation, a very fast propagation of the vortex core towards the opposite side of nanostripe occurs [Fig. 7(c)]. The last configuration remains stable at negative fields up to -390 Oe [Fig. 9(g)] when the Néel domains disappear. Notice the difference in the size of the domain.

B. Influence of defects on magnetization in PER nanostripes

Defects are known to act as preferential nucleation sites for domain walls—thus decreasing the coercive fields in single domain samples—and also as pinning centers for moving domain walls. In the present work, the influence of the defects in nanostripes has been studied both theoretically and experimentally.

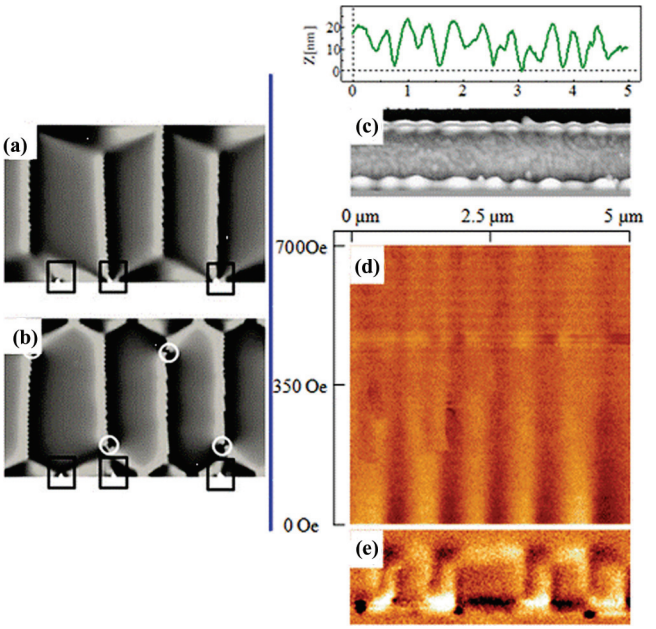

FIG. 10. (Color online) Results of the micromagnetic simulation for PER nanostripe, introducing very small edge defects: (a) before vortex nucleation; (b) after vortex nucleation. The color is the divergence of the magnetization vector, the open circles are the positions of vortex cores in DWs, and open squares are the positions of edge defects. (c) Experimental topography, profile along the marked line, and (d) the 3D mode image of the PER750 nanostripe corresponding to the magnetic state evolution as a function of the externally applied magnetic field from $+700$ to 0 Oe. (e) MFM image of the nanostripe after the 3D mode experiment.

First, simulations have been performed introducing very small edge defects in the lateral sides of PER nanostripes. The simulations have shown that during the magnetization reversal process and just before the vortex formation, defects can pin 180° DWs, leading to nonperiodic domain structure [see Fig. 10(a)]. However, the consequent vortex formation and its propagation are independent on the position of the pining defects as can be observed in Fig. 10(b).

In order to study this effect, an original experiment was carried out involving a 3D-mode measurement along one long edge of the stripes. Figure 10(c) shows the topographic map of the PER750 stripe. The dark blue line corresponds to the profile along which the tip is continuously scanned, and after every single scan an external field along the main axis is swept.

Figure 10(d) shows a 3D-mode image under the explained configuration, from positive saturation down to remanence.

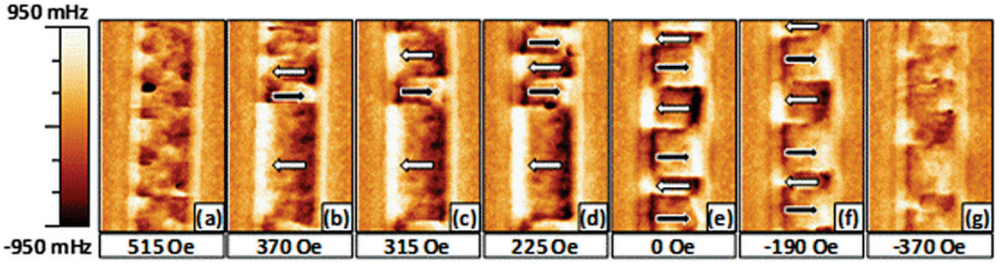

FIG. 9. (Color online) MFM images obtained in PER850 at different magnetic fields applied along the main axis.

As can be seen for large fields, the domain walls have preferential nucleation sites attributed to structural defects. As the field is decreased, some of these walls move or even annihilate because of the decreasing influence of those defects in comparison to the magnetocrystalline anisotropy, as the simulations predict. As a result, the domain wall position, even though influenced by the region where it was formed, does not always correspond to its nucleation site. Finally, in the remanent state the asymmetric domain configuration is again obtained, as observed both in Figs. 10(d) and 10(e). Notice the similarity in the contrast between the lower part of Fig. 10(d) and the upper part of Fig. 10(e), where the 3D-mode measurement was performed. It is worth remarking that the position of the domain walls at remanence is statistically reproducible.

VI. CONCLUSION

We have studied epitaxial Co(111) nanostripes with strong uniaxial magnetic anisotropy, induced by the vicinal Si(111) substrate, using MOKE, VF-MFM, and micromagnetic simulations. All those experiments and simulations allow us to offer a detailed description and explanation of the hysteresis processes, the corresponding magnetization configurations, and DW structure. Two kinds of nanostructures (so-called PAR and PER) have been fabricated regarding the easy axis direction of both magnetocrystalline and shape anisotropies. In addition, the aspect ratio of the nanostripes varies in order to tune the influence of the shape anisotropy. The PAR nanostripes present uniaxial anisotropy since both the magnetocrystalline and the shape anisotropies point along the longitudinal direction. However, the PER nanostripes—where the shape anisotropy competes with the uniaxial magnetocrystalline anisotropy—exhibit richer magnetic behavior. Metastable transverse single domain states can be stabilized in the widest PER nanostripes by applying magnetic field along the long axes, reflecting that the overall anisotropy is directed perpendicular to it. In this case we have identified the compensation region, the width of nanostripes for which the shape anisotropy compensates the magnetocrystalline anisotropy. In this region both transverse single domain and open stripe domain structures coexist. The combination of the VF-MFM measurements, including the so-called 3D mode MFM-based technique, and the micromagnetic simulations have allowed us to identify the types of DWs during the magnetization reversal as 180 Néel walls (OS state, before the vortex formation), containing "vortex" walls (OSD state) and double "vortex" structures for wide PER nanostripes. The prediction of the micromagnetic simulations about the change of the contrast of the domain walls under an applied field due to the vortex propagation has been confirmed by VF-MFM imaging. The defects are shown to be responsible for DW pinning but to have smaller influence on the vortex formation. The nanostructures presented in this work offer an additional possibility to control the magnetic structure via their geometry which may constitute a valuable property for future applications.

ACKNOWLEDGMENTS

The authors acknowledge the financial support from the Spanish Ministry of Economy and Competitivity under Projects No. CSD2010-00024, No. FIS2010-20979-C02-02, and No. MAT2010-20798-C05-01, and Fellowship No. SB2010-0123, provided to. Y. Ivanov as well as the financial support from the regional Government of Madrid under Project No. S2009MAT-1467.

[1] L. Thomas, M. Hayashi, R. Moriya, C. Rettner, and S. Parkin, Nat. Commun. **3**, 810 (2012).
[2] D. A. Allwood, G. Xiong, C. C. Faulkner, D. Atkinson, D. Petit, and R. P. Cowburn, Science **309**, 1688 (2005).
[3] S. S. P. Parkin, M. Hayashi, and L. Thomas, Science **320**, 190 (2008).
[4] J. Topp, D. Heitmann, M. P. Kostylev, and D. Grundler, Phys. Rev. Lett. **104**, 207205 (2010).
[5] D. A. Allwood, G. Xiong, M. D. Cooke, C. C. Faulkner, D. Atkinson, N. Vernier, and R. P. Cowburn, Science **296**, 2003 (2002).
[6] E. R. Lewis, D. Petit, L. O'Brien, A. Fernandez-Pacheco, J. Sampaio, A.-V. Jausovec, H. T. Zeng, D. E. Read, and R. P. Cowburn, Nat. Mater. **9**, 980 (2010).
[7] M. Kläui, P.-O. Jubert, R. Allenspach, A. Bischof, J. A. C. Bland, G. Faini, U. Rüdiger, C. A. F. Vaz, L. Vila, and C. Vouille, Phys. Rev. Lett. **95**, 026601 (2005).
[8] M. Kläui, C. A. F. Vaz, J. A. C. Bland, L. J. Heyderman, F. Nolting, A. Pavlovska, E. Bauer, S. Cherifi, S. Heun, and A. Locatelli, Appl. Phys. Lett. **85**, 5637 (2004).
[9] A. D. Kent, J. Yu, U. Rudiger, and S. S. P. Parkin, J. Phys.: Condens. Matter **13**, R461 (2001).
[10] C. L. Dennis, R. P. Borges, L. D. Buda, U. Ebels, J. F. Gregg, M. Hehn, E. Jouguelet, K. Ounadjela, I. Petej, I. L. Prejbeanu, and M. J. Thornton, J. Phys.: Condens. Matter **14**, R1175 (2002).
[11] U. Ruediger, J. Yu, S. Zhang, A. D. Kent, and S. S. P. Parkin, Phys. Rev. Lett. **80**, 5639 (1998).
[12] C. Hassel, F. M. Römer, R. Meckenstock, G. Dumpich, and J. Lindner, Phys. Rev. B **77**, 224439 (2008).
[13] A. Biehler, M. Kläui, M. Fonin, C. König, G. Güntherodt, and U. Rüdiger, Phys. Rev. B **75**, 184427 (2007).
[14] S. Cherifi, R. Hertel, A. Locatelli, Y. Watanabe, G. Potdevin, A. Ballestrazzi, M. Balboni, and S. Heund, Appl. Phys. Lett. **91**, 092502 (2007).
[15] G. Leaf, H. Kaper, M. Yan, V. Novosad, P. Vavassori, R. E. Camley, and M. Grimsditch, Phys. Rev. Lett. **96**, 017201 (2006).
[16] E. R. Lewis, D. Petit, A.-V. Jausovec, L. O'Brien, D. E. Read, H. T. Zeng, and R. P. Cowburn, Phys. Rev. Lett. **102**, 057209 (2009).
[17] D. A. Allwood, T. Schrefl, G. Hrkac, I. G. Hughes, and C. S. Adams, Appl. Phys. Lett. **89**, 014102 (2006).
[18] P. Vavassori, V. Metlushko, B. Ilic, M. Gobbi, M. Donolato, M. Cantoni, and R. Bertacco, Appl. Phys. Lett. **93**, 203502 (2008).

[19] A. Torti, V. Mondiali, A. Cattoni, M. Donolato, E. Albisetti, A. M. Haghiri-Gosnet, P. Vavassori, and R. Bertacco, Appl. Phys. Lett. **101**, 142405 (2012).

[20] L. O'Brien, D. Petit, H. T. Zeng, E. R. Lewis, J. Sampaio, A. V. Jausovec, D. E. Read, and R. P. Cowburn, Phys. Rev. Lett. **103**, 077206 (2009).

[21] M. Negoita, T. J. Hayward, and D. A. Allwood, Appl. Phys. Lett. **100**, 072405 (2012).

[22] A. V. Davydenko, Yu. P. Ivanov, and L. A. Chebotkevich, J. Magn. Magn. Mater. **324**, 1248 (2012).

[23] W. Scholz, J. Fidler, T. Schrefl, D. Suess, R. Dittrich, H. Forster, and V. Tsiantos, Comput. Mater. Sci. **28**, 366 (2003).

[24] M. Donahue and D. Porter, Object Oriented Micromagnetic Framework (OOMMF) The National Institute of Standards and Technology (NIST), http://math.nist.gov/oommf/, 2006.

[25] M. Jaafar, J. Gómez-Herrero, A. Gil, P. Ares, M. Vázquez, and A. Asenjo, Ultramicroscopy **109**, 693 (2009).

[26] M. Jaafar, L. Serrano-Ramón, O. Iglesias-Freire, A. Fernández-Pacheco, R. M. Ibarra, J. M. De Teresa, and A. Asenjo, Nanoscale Res. Lett. **6**, 407 (2011).

[27] Yu. P. Ivanov, A. I. Ilin, A. V. Davydenko, and A. V. Zotov, J. Appl. Phys. **110**, 083505 (2011).

[28] I. V. Roshchin, J. Yu, A. D. Kent, G. W. Stupian, and M. S. Leung, IEEE Trans. Magn. **37**, 2101 (2001).

[29] Micromagnetic simulations corresponding to the magnetization reversal along the easy axis of both kinds of nanostripes performed by MAGPAR introducing very small edge defects (size $0.02w$ and periodicity $0.03l$) show a significant reduction of the simulated coercivity values.

[30] R. C. O'Handley, *Modern Magnetic Materials: Principles and Applications* (John Wiley & Sons, New York, 2000), p. 740.

[31] F. Garcia-Sanchez, O. Chubykalo-Fesenko, A. Martinez, and J. M. Gonzalez, Physica B **403**, 469 (2008).

[32] http://www.nanotec.es.

[33] O. Iglesias-Freire (unpublished).